A search for ultrahigh-energy neutrinos associated with astrophysical sources using the third flight of ANITA

ANITA Collaboration

C. Deaconu[a] L. Batten[b] P. Allison[c] O. Banerjee[c] J. J. Beatty[c]
K. Belov[d] D. Z. Besson[e,f] W. R. Binns[g] V. Bugaev[g] P. Cao[h]
C. H. Chen[i] P. Chen[i] Y. Chen[i] J. M. Clem[h] A. Connolly[c]
L. Cremonesi[j] B. Dailey[c] P. F. Dowkontt[g] B. D. Fox[k]
J. W. H. Gordon[c] P. W. Gorham[k] C. Hast[l] B. Hill[k] S. Y. Hsu[i]
J. J. Huang[i] K. Hughes[a,c] R. Hupe[c] M. H. Israel[g] K. M. Liewer[d]
T. C. Liu[i] A. B. Ludwig[a] L. Macchiarulo[k] S. Matsuno[k]
K. McBride[c] C. Miki[k] K. Mulrey[h] J. Nam[i] C. Naudet[d]
R. J. Nichol[b] A. Novikov[e,f] E. Oberla[a] S. Prohira[c,e] R. Prechelt[k]
B. F. Rauch[g] J. Ripa[i] J. M. Roberts[k,m] A. Romero-Wolf[d]
B. Rotter[k] J. W. Russell[k] D. Saltzberg[n] D. Seckel[h]
H. Schoorlemmer[k] J. Shiao[i] S. Stafford[c] J. Stockham[e]
M. Stockham[e] B. Strutt[n] M. S. Sutherland[c] G. S. Varner[k]
A. G. Vieregg[a] N. Wang[n] S. H. Wang[i] S. A. Wissel[o]

[a]Dept. of Physics, Enrico Fermi Inst., Kavli Inst. for Cosmological Physics, Univ. of Chicago, Chicago, IL 60637.

[b]Dept. of Physics and Astronomy, University College London, London, United Kingdom.

[c]Dept. of Physics, Center for Cosmology and AstroParticle Physics, Ohio State Univ., Columbus, OH 43210.

[d]Jet Propulsion Laboratory, California Institute for Technology, Pasadena, CA 91109.

[e]Dept. of Physics and Astronomy, Univ. of Kansas, Lawrence, KS 66045.

[f]Moscow Engineering Physics Institute, Moscow, Russia.

[g]Dept. of Physics, McDonnell Center for the Space Sciences, Washington Univ. in St. Louis, MO 63130.

[h]Dept. of Physics, Univ. of Delaware, Newark, DE 19716.

[i]Dept. of Physics, Grad. Inst. of Astrophys., Leung Center for Cosmology and Particle Astrophysics, National Taiwan University, Taipei, Taiwan.

^{j}School. of Physics and Astronomy, Queen Mary University of London, London, United Kingdom.

^{k}Dept. of Physics and Astronomy, Univ. of Hawaii, Manoa, HI 96822.

^{l}SLAC National Accelerator Laboratory, Menlo Park, CA, 94025.

^{m}Center for Astrophysics and Space Sciences, Univ. of California, San Diego, La Jolla, CA 92093.

^{n}Dept. of Physics and Astronomy, Univ. of California, Los Angeles, Los Angeles, CA 90095.

^{o}Physics Dept., Pennsylvania State Univ., State College, PA 16802.

E-mail: cozzyd@kicp.uchicago.edu

Abstract. The ANtarctic Impulsive Transient Antenna (ANITA) long-duration balloon experiment is sensitive to interactions of ultra high-energy ($E > 10^{18}$ eV) neutrinos in the Antarctic ice sheet. The third flight of ANITA, lasting 22 days, began in December 2014. We develop a methodology to search for energetic neutrinos spatially and temporally coincident with potential source classes in ANITA data. This methodology is applied to several source classes: the TXS 0506+056 blazar and NGC 1068, the first potential TeV neutrino sources identified by IceCube, flaring high-energy blazars reported by the Fermi All-Sky Variability Analysis, gamma-ray bursts, and supernovae. Among searches within the five source classes, one candidate was identified as associated with SN 2015D, although not at a statistically significant level. We proceed to place upper limits on the source classes. We further comment on two subthreshold events and potential application of this methodology to more sensitive future instruments.

Contents

1 Introduction

The Antarctic Impulsive Transient Antenna (ANITA) experiment [1] deploys a balloon-borne radio interferometer to search for the impulsive Askaryan radio emission [2, 3] expected to be produced by the interactions of ultrahigh-energy (UHE) neutrinos ($E > 10^{18}$ eV) interacting in polar ice. ANITA has previously reported constraints on diffuse UHE neutrinos [4–7] as well as neutrinos in time-coincidence with gamma-ray bursts (GRBs) [8]. So far, no candidate events have been observed above background expectations in the Askaryan channel, but the ANITA program sets the most stringent limits on the diffuse UHE flux at energies above $10^{19.5}$ eV.

Cosmogenic UHE neutrinos are expected to be produced in the interactions of the UHE cosmic-rays (UHECR) with the CMB (i.e. the GZK process) [9–11]. The sources of the UHECR are unknown, and it is also not known if the sources are transient in nature or steady-state. Typical GZK interaction lengths of a few hundred Mpc imply cosmogenic neutrinos will retain the source direction over cosmological distances, but it is likely that time association with potential astrophysical transients will be lost due to deflections of UHECR by intergalactic magnetic fields.

Astrophysical neutrinos, believed to be produced directly in astrophysical sources, have been detected at TeV-PeV energies by IceCube [12]. IceCube has identified evidence for some particular astrophysical neutrino sources, including TXS 0506+056 [13, 14] and NGC 1068 [15]. Astrophysical neutrinos may also exist at UHE energies, either as a continuation
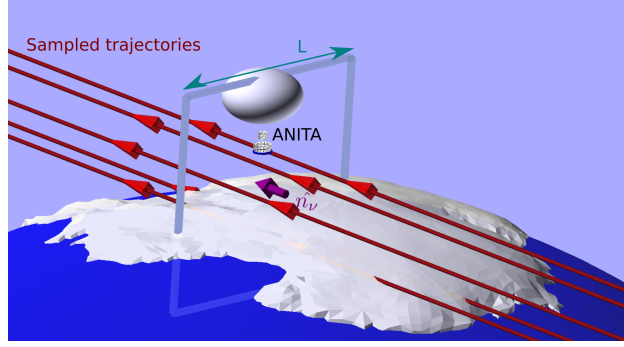
Figure 1. An illustration of the sampling method used for the point-source simulation. See text for details.

of the same flux that IceCube has detected, or from other sources, such as flat-spectrum radio quasars (FSRQs) [16, 17] or GRBs [18].

Compared to a diffuse UHE neutrino search, a search for UHE neutrinos associated with particular sources can narrow the detection phase space in direction and, for transient objects, in time. This in general allows a reduction in backgrounds and/or an improvement in analysis efficiency, therefore increasing the sensitivity compared to diffuse fluxes.

In this paper, we build on an ANITA-III diffuse search to develop a methodology to search for UHE neutrinos in spatial and time coincidence with astrophysical source classes. We define a source class as a specification of the time-dependent neutrino flux from one or more sources, $\mathbf{F}(E,t) = \sum_{\text{sources}} F_i(E,t)$. This methodology is applied to the ANITA-III flight for five source classes: TXS 0506+056, NGC 1068, blazars flaring in UHE gamma-rays as identified by the Fermi All-sky Variability Analysis (FAVA [19]), GRBs, and supernovae (SN).

2 Simulation

The standard ANITA simulation, `icemc` [20], is designed for efficient simulation of a diffuse flux of neutrinos. The default volumetric sampling scheme is very efficient in sampling neutrinos likely to trigger ANITA, but is not appropriate for modeling point sources, as it relies on the "thin target" approximation, converting effective volume to effective area by dividing by the interaction length. As such, a new sampling scheme was developed for this search within `icemc`.

The first step is to choose a payload position/time and neutrino direction. A random time is chosen within the ANITA-III flight which determines the payload position and orientation. The neutrino direction is chosen based on the simulated parameters, for example, a single source, an isotropic flux, or from a collection of time-varying sources.

For a given payload position, $\vec{x}_{\text{ANITA}}$, and neutrino direction, $\hat{p}_\nu$, a straightforward way to calculate the effective area for a given neutrino energy, E_ν, is to consider a square with side L, normal to $\hat{p}_\nu$ and throw neutrinos with random trajectories passing through the square (see Figure 1). Assuming that the square is centered near $\vec{x}_{\text{ANITA}}$ (we center it at the ice surface below ANITA) and L is large enough that all neutrinos that trigger ANITA intersect the sampling box, the trigger-level effective area for that configuration is then:

$$A_{\text{eff}}(\hat{p}_\nu, \vec{x}_{\text{ANITA}}, E_\nu) = L^2 \frac{n_{\text{trigger}}}{n_{\text{thrown}}}. \tag{2.1}$$

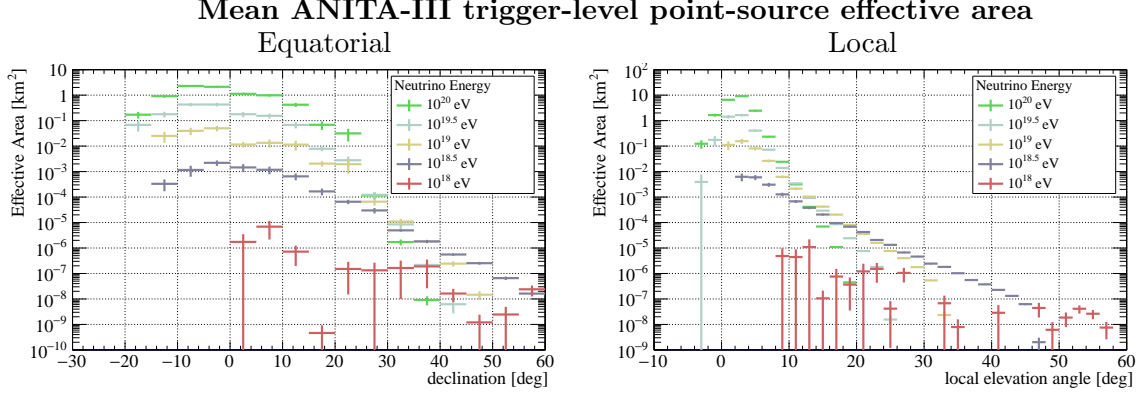## Mean ANITA-III trigger-level point-source effective area

Figure 2. The point-source effective area as a function of declination (left) or local elevation angle (right) averaged over the ANITA-III flight at several energies. Errors shown are statistical only. Local elevation angle is measured downward from payload horizontal. Because ANITA moves slowly compared to the diurnal cycle, the flight-averaged acceptance is nearly constant with α. The total flight time is 22 days. The point-source simulation results here cannot be directly compared to the diffuse sensitivities quoted elsewhere by ANITA as those are typically geometric averages of multiple independent codes.

A value of $L = 1200$ km is a conservative choice that will miss no events for ANITA-III.

This can readily be generalized to calculating ANITA's effective area of a point source with sky position Θ by choosing the appropriate $\hat{p}_\nu$ at each sampled $\vec{x}_{\mathrm{ANITA}}$, integrating over the flight trajectory by uniformly choosing random times within the flight:

$$A_{\mathrm{eff}}(\Theta, E_\nu) = L^2 \frac{n_{\mathrm{trigger}}}{n_{\mathrm{thrown}}}. \tag{2.2}$$

The remaining difficulty is efficiently calculating n_{trigger}. The naive forward calculation, which involves propagating a neutrino through the Earth until it interacts or exits and checking if ANITA triggers for interacting neutrinos, is computationally wasteful. Instead, the following scheme is used:

1. Check if the neutrino trajectory intersects an ellipsoid defined by the geodesic reference ellipsoid plus 5 km (the highest altitude in Antarctica is 4,892 m). If not, there is no chance of detection, so skip to the next event.

2. Find the intersection points of the neutrino with the Antarctic ice volume (as defined by BEDMAP2 [21]). A step size of 50 m is used in order to detect intersections with ice at least that small. If no intersection with ice is detected, then we have no chance of detecting this neutrino, so skip to the next event.

3. In general, there may be multiple intersections with the ice. For each intersecting segment, we calculate a weight, w_s, that is the product of the probability of the neutrino interacting within ice segment and the probability that the neutrino did not interact in the Earth prior to reaching the segment.

4. We choose one intersecting segment at random, and pick an interaction point within that segment with an exponential distribution. We correspondingly multiply w_s by the number of intersecting segments to compensate.

5. We then proceed with the rest of the simulation as usual (e.g. pick interaction type from differential cross-section, sample inelasticity, etc.) and evaluate if ANITA triggers on the radio emission.

6. We now define n_{trigger} as the sum of w_s for events that trigger.

This method can also be used to simulate a diffuse flux by choosing the source direction at random in each trial, effectively performing a Monte Carlo integral over $d\Omega$. By doing so, we can compare to the traditional `icemc` sampling method and find that the diffuse effective areas agree for ANITA-III at the 20% level, which we consider an acceptable level of agreement, subdominant to other systematic errors in the simulation [20]. The time-averaged point-source UHE neutrino effective areas as a function of declination and elevation angles over the ANITA-III flight are shown in Figure 2.

Finally, and crucially, this method may easily be adapted to simulate ANITA's response to a source class. We integrate over the flight trajectory by sampling times during the flight. At each time, we draw from the sources active at the time with probability proportional to its relative flux compared to all other active sources and apply an additional time-dependent weight $w_t = \mathbf{F}(E,t)/\int_{t_0}^{t_1} \mathbf{F}(E,t)dt$.

3 Source Search Methodology

We adapt Analysis B from the ANITA-III diffuse search, which is described in detail in the appendices of [6]. A brief review is provided here.

3.1 Review of diffuse ANITA analysis

Whenever ANITA triggers, an event is formed from 96 100-ns-long waveforms digitized from 48 dual-polarization antennas with known relative positions and time delays. These waveforms are filtered to remove narrow-band contamination, then an interferometric map is generated for each polarization, where the mean cross-correlation between antennas is computed as a function of elevation and azimuth in payload-centric coordinates. Directions corresponding to the peaks of these maps are considered hypotheses and coherently-summed waveforms are created in those directions, from which various observables are computed. Analysis B applies three sets of cuts to select diffuse neutrino and air shower candidates:

1. Quality Cuts ($\mathcal{Q}$), to remove digitizer glitches, radio interference from the payload itself, and other problematic events.

2. A Fisher discriminant, ($\mathcal{F}$), selecting for neutrino-like events. This multivariate discriminant is constructed using a variety of observables from event waveforms (e.g. cross-correlation, coherence, signal size, impulsivity, linear polarization) and is trained on a sample of thermal events and simulation, to select impulsive broadband events.

3. A spatial isolation parameter, $\mathcal{O}$, based on projecting events to the continent, to remove likely anthropogenic events. This parameter is equal to the overlap integral of each event's pointing resolution projected onto the continent with that of other events. Only events with sufficiently high $\mathcal{F}$ are included in this integral, with a soft turn-on (so that events less likely to be neutrino-like are given a smaller weight). As $\mathcal{O}$ quickly becomes very small for events that are far apart, it is convenient to set cuts on $-\log_{10}\mathcal{O}$ instead of $\mathcal{O}$ directly.
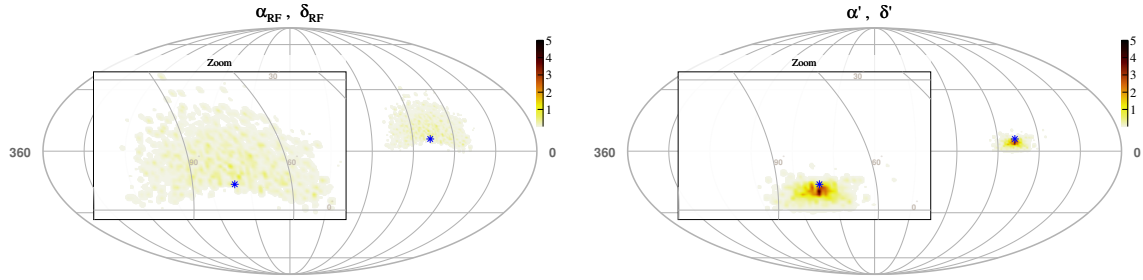
Figure 3. The distribution in equatorial coordinates of the apparent RF direction (left) for simulated neutrinos from TXS 0506+056, and the reconstructed neutrino direction (right) using the approximate reconstruction method described in the text. The more compact distribution allows for improved background discrimination. The color axis depicts the percentage of spatial distribution within each angular bin; bins contributing less than 0.01 percent are not shown for clarity. As one measure of the improvement in localization, the standard deviation in α improves from 13.3 degrees to 4.5 degrees and the standard deviation in δ improves from 6.4 degrees to 1.7 degrees.

Emission from neutrinos at the payload is primarily vertically-polarized due to the typically-skimming geometry of UHE neutrinos and preferential transmission at the ice-air interface, so only predominantly vertically-polarized are considered neutrino candidates. $\mathcal{Q}$ was optimized to reduce the number of poor-quality events to a negligible level and then $\mathcal{F}$ and $\mathcal{O}$ each had cut values optimized for sensitivity to a diffuse flux. The primary contribution to the background estimate is anthropogenic, with negligible background from thermal noise, glitches and payload-generated radio interference.

3.2 $\mathcal{D}$, the source class distance

We now develop a methodology to optimize the search for sensitivity to a given source class rather than a diffuse flux. For expedience, we will keep the definitions of $\mathcal{Q}$, $\mathcal{O}$ and $\mathcal{F}$, but introduce a new "source distance" parameter, $\mathcal{D}$, specialized for a given source class. We will then optimize cut values for $\mathcal{F}$, $\mathcal{O}$ and $\mathcal{D}$ to maximize search sensitivity. The $\mathcal{Q}$ cut values are kept the same as in the diffuse analysis.

Interferometric event reconstruction produces an estimated direction of the radio emission (ϕ_{RF}, θ_{RF}) in payload coordinates. Since the orientation, time and position of the payload at each event is known, this can be projected into equatorial coordinates, right ascension (α) and declination (δ). Using simulation, these sky distributions of (α_{RF}, δ_{RF}) may be estimated for a neutrino flux.

While this simple method could be used as the basis of a source distance cut, due to the opening angle of the in-ice Cerenkov cone, these distributions are not compact (see Figure 3, left), which reduces the ability to efficiently reject background. One way to reduce this dispersion is to estimate the neutrino direction. Because the Askaryan emission is radially-polarized, the observed polarization state of the radio emission from neutrino is related to the neutrino direction. However, this is complicated by instrumental and radio propagation effects and convolved with earth attenuation. The spectrum of the event additionally gives some information about how off-cone the observation is.

For a putative ANITA neutrino candidate, the most robust (albeit model-dependent, as an energy spectrum must be assumed) way of estimating the neutrino direction is to simulate neutrinos from different directions with the payload fixed at the observation location and then determine which neutrino directions are most compatible with the observed RF direc-

tion, polarization, and signal spectrum. However, while doable for an interesting candidate, it is computationally infeasible to use this procedure in a search. Moreover, the primary purpose here is not to reconstruct the most likely neutrino direction, but instead to improve background rejection by constructing a more compact observable. Systematic biases in the direction are not problematic as long as they are present in both data and simulation.

To this end, a large set of isotropically-distributed neutrinos were simulated at various energies and run through the same reconstruction framework as data. TMVA [22] was used to regress a polynomial for $\Delta\phi = \phi_\nu - \phi_{RF}$ and $\Delta\theta = \theta_\nu - \theta_{RF}$ as a function of a number of observables, including the observed coherent waveform polarization state, spectral parameters, signal size, and θ_{RF}. By applying this regression to each event, we can compute an estimator for $\Delta\phi$ and $\Delta\theta$ and therefore the neutrino direction. With knowledge of the payload position and orientation, this can then be projected to our equatorial coordinate estimators (α', δ'). We can test the improved compactness of the estimator by applying the reconstruction to Monte Carlo truth, as shown in Figure 3, right. We find an improvement dispersion for the estimator of a factor of 3-4 in each of α' and δ'.

In order to define a source distance parameter in as generic a way as possible, without any assumptions about the shape or modality of the distribution, we use a data-driven histogramming approach. We simulate neutrinos from a source class, process the simulated events, and run the estimator regression to generate a three-dimensional *exposure histogram* with axes of reconstructed α', δ', and event time. For a steady source class, the time axis is extraneous and may be ignored. In the case of discrete source turn-on and turn-off times, it is convenient to choose the time bins to align with transitions. This exposure histogram is then converted to an *exposure percentile histogram*, where each bin's value is computed as fraction of the total exposure with differential exposure greater than the differential exposure of the bin (e.g. Figure 4). This results in a histogram where the bins with the highest exposure to the source class have values close to 0 and bins with poor or no exposure have a values close to 1. We finally define $\mathcal{D}$ for an event as the value of this exposure percentile histogram for its α', δ' and event time. This definition has the convenient property that setting the cut on
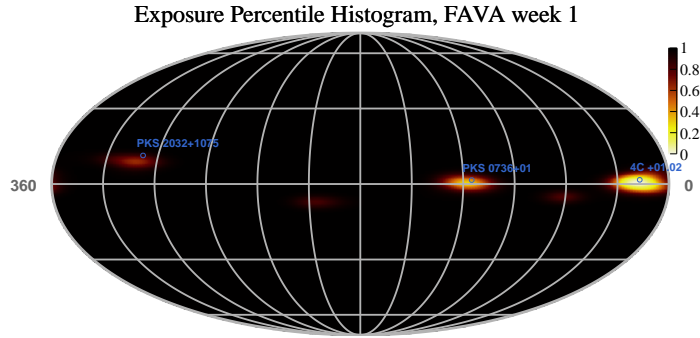

Figure 4. An example time slice of an *exposure percentile histogram*, in this case for the first week of FAVA-detected flaring blazars, which contains multiple sources of varying exposure. The value at each point (α', δ', t) is set to the fraction of the total exposure with differential exposure higher than the differential exposure at the point, so that lower values represent regions of greater exposure. A cut in $\mathcal{D}$ defines the region in (α', δ', t) with value smaller than the cut value, preferentially selecting regions with the greatest exposure density. The sources corresponding to the three highest-exposure regions are labeled, although note that in general there may be an offset between the coordinate estimator and the actual source coordinates.

$\mathcal{D}$ to a value $d \in [0,1]$ roughly selects the highest exposure density and has an efficiency to events from that source class of approximately d.

One technical aspect of $\mathcal{D}$ was deferred until now. Because it is very time-consuming to generate enough simulated events to smoothly fill this exposure histogram at fine resolution, we start with a relatively coarsely binned α' and δ' axes and then use a kernel density estimator in each time slice to create a smoother, more finely-binned histogram. The kernel density estimator scale parameters are tuned so that the distribution of $\mathcal{D}$ for members of the source class is roughly uniform. Small deviations from uniformity are of little concern as long as there is sufficient dynamic range in efficiency versus $\mathcal{D}$ to effectively scan the parameter. To reduce bias, disjoint sets of simulated data are used to create the estimator and for cut optimization, described next.

3.3 Cut Optimization

For each source class, we seek to set optimal cuts in a blind way on the $\mathcal{F}$ (the signal-likeness parameter), $\mathcal{O}$ (the spatial isolation parameter) and $\mathcal{D}$ (the source class distance parameter). We scan in these parameters to optimize expected sensitivity, using:

$$\text{sens.} \propto \left\langle \frac{\text{FC}_{90}\left(\text{Pois}\left(\mu_{\text{BG}}\right), \mu_{\text{BG}}\right)}{\epsilon} \right\rangle, \tag{3.1}$$

where μ_{BG} is the background estimate for a given set of cuts, ϵ is the expected analysis efficiency for a given set of cuts (the fraction of events that trigger ANITA that also pass analysis cuts), Pois is the Poisson distribution and FC_{90}(sig,bg) is the 90% Feldman-Cousins upper limit factor [23] for a given number of signal events and background events. The mean is taken here because both μ_{bg} and ϵ have uncertainties, which are integrated over using the semi-Bayesian Cousins-Highland method [24].

The estimate for analysis efficiency for a given set of cuts may readily be estimated from simulation by simply applying the same cuts to simulated data. A Gaussian systematic error of 10% on the analysis efficiency is assumed, as used in the diffuse analysis.

To estimate the background as a function of cut values, we use a data-driven on-off [25] approach based on time shuffling. For each event passing a trial $\mathcal{F}$ and $\mathcal{O}$, we shift the event time by a random offset between 1.5 hours and 22.5 hours (in either direction) 100 times. These bounds are set so that a significantly different right ascension is guaranteed while preserving some time locality. For each resampling time, we count how often the cut on $\mathcal{D}$ is passed in this off-time sideband (which is approximately seven times larger in phase space than the "on-time" region). The posterior on the background estimate is then conservatively taken to be the Poisson posterior using a uniform prior for a sideband seven times larger:

$$p(\mu_{BG}) = \Gamma(7N_{pass}/100 + 1, 1/7). \tag{3.2}$$

This method is somewhat limited by the statistics of the sideband. As soon as the cuts are so stringent that N_{pass} becomes zero, the background estimate will always be the same $(0.10^{+0.16}_{-0.07})$, no matter how much more the cuts are tightened. Consideration of the efficiency in the sensitivity will typically shift the optimization to the boundary, somewhat alleviating this problem. An alternative would require a different strategy such as imposing a background model, which is difficult for the time-varying anthropogenic backgrounds faced by ANITA. A different choice of prior (e.g. Jeffreys) would also reduce the background estimate at the cost of non-conservative coverage.

Using this methodology, we can perform a three-dimensional scan over reasonable parameters of $\mathcal{F}$, $-\log_{10}\mathcal{O}$ and $\mathcal{D}$ to choose cuts that optimize our sensitivity metric for any particular source class. Finally, as in the diffuse search, we only select events that are more impulsive in vertical polarization (VPol) than horizontal polarization (HPol) to avoid selecting air shower events.

4 Sources considered

Having developed an appropriate methodology, we now turn our attention to potentially interesting sources for ANITA-III. Sources of the same type are pooled together into a single source class in order to reduce the global trials factor. This requires some model dependence in choosing the analysis cuts, but once cuts are chosen, model-independent limits may be placed on each source within the class. These limits may not be optimal for any given model other than the one used to set cuts, but we make an attempt to adopt a "least-common denominator" set of cuts to minimize the model-dependence.

Each search is optimized and performed independently, but the significance of any particular search's result must be interpreted in the context of the number of searches performed. We considered optimizing for a global 90% significance (which is roughly equivalent to setting a higher optimized significance in each search, if they are weighted equally), but found that this did not strongly affect where the optimized cuts are placed and we did not want to restrict the possibility of any additional future searches. It is also possible for a given event to be considered a candidate by multiple searches. The considered objects are tabulated in Table 1 and the result of each optimization is shown in Table 2.

4.1 TXS 0506+056

The TXS 0506+056 blazar has been identified by IceCube as a potential source of astrophysical neutrinos. This association is due to a gamma-ray flare in spatial and temporal coincidence with a September 22, 2017 likely astrophysical neutrino candidate that triggered a multi-messenger alert [13]. Afterwards, archival data suggested an excess of neutrinos from the direction of TXS 0506+056 in a several-month window around December 2014 [14], albeit without any gamma-ray activity in the blazar [26]. The ANITA-III flight coincided temporally with this earlier neutrino "burst" and TXS 0506+056, at a declination of 5.6 degrees, is within ANITA-III's sensitive field-of-view, motivating a dedicated search.

IceCube has measured a spectral index for the neutrino burst of $\gamma = 2.1 \pm 0.2$. To optimize cuts for the ANITA-III search, we simulate neutrinos from the direction of TXS 0506+056 with $\gamma = 2$, which is compatible with the IceCube measurement and somewhat preferred theoretically. The optimization results in an estimated analysis efficiency to an E^{-2} flux of 91.7% with a background estimate of $0.10^{+0.16}_{-0.07}$, which is the minimal background estimate calculable with the method employed (i.e. zero passing sideband events).

4.2 NGC 1068

IceCube has identified NGC 1068 as a potential neutrino point source [15] at the 2.9σ level. IceCube does not report any temporal information for NGC 1068, and the best-fit spectral index (3.2) from IceCube would make detection by ANITA-III unlikely. However, as it is one of two just objects within ANITA's field of view that has been identified as a potential high-energy neutrino source at this significance level, a search is justified.

<p align="center">**Objects Considered**</p>

Object	Search	Coordinates	Times Considered (UTC)
TXS 0506+056	TXS 0506+056	$\alpha = 77.4°, \delta = 5.7°$	Full Flight
NGC 1068	NGC 1068	$\alpha = 40.7°, \delta = -0.0°$	Full Flight
3C 454.3	Flaring Blazar	$\alpha = 344°, \delta = 16.1°$	2014-12-15-15:43:38Z + 1 week
4C +01.02	Flaring Blazar	$\alpha = 17°, \delta = 1.6°$	2014-12-15-15:43:38Z + 4 weeks
* B3 1343+451	Flaring Blazar	$\alpha = 206°, \delta = 44.8°$	2015-01-05-15:43:38Z + 1 weeks
CTA 102	Flaring Blazar	$\alpha = 331°, \delta = 11.7°$	2014-12-22-15:43:38Z + 3 weeks
MG1 J221916+1806	Flaring Blazar	$\alpha = 335°, \delta = 18.0°$	2014-12-15-15:43:38Z + 2 weeks
* PKS 0402-362	Flaring Blazar	$\alpha = 61°, \delta = -36.0°$	2014-12-15-15:43:38Z + 4 weeks
PKS 0502+049	Flaring Blazar	$\alpha = 76°, \delta = 5.0°$	2014-12-22-15:43:38Z + 3 weeks
PKS 0736+01	Flaring Blazar	$\alpha = 115°, \delta = 1.5°$	2014-12-15-15:43:38Z + 2 weeks
PKS 1441+25	Flaring Blazar	$\alpha = 221°, \delta = 25.0°$	2014-12-15-15:43:38Z + 4 weeks
PKS 1717+177	Flaring Blazar	$\alpha = 260°, \delta = 17.7°$	2014-12-22-15:43:38Z + 2 weeks
* PKS 1830-211	Flaring Blazar	$\alpha = 278°, \delta = -21.1°$	2015-01-05-15:43:38Z + 1 weeks
PKS 2032+1075	Flaring Blazar	$\alpha = 309°, \delta = 10.9°$	2014-12-15-15:43:38Z + 1 weeks
* PKS 2052-47	Flaring Blazar	$\alpha = 314°, \delta = -47.3°$	2014-12-22-15:43:38Z + 2 weeks
* PKS 2142-75	Flaring Blazar	$\alpha = 327°, \delta = -75.7°$	2014-12-15-15:43:38Z + 1 weeks
PKS B1319-093	Flaring Blazar	$\alpha = 200°, \delta = -9.3°$	2014-12-15-15:43:38Z + 1 weeks
* PMN J2141-6411	Flaring Blazar	$\alpha = 325°, \delta = -64.2°$	2014-12-29-15:43:38Z + 1 weeks
RGB J2243+203	Flaring Blazar	$\alpha = 341°, \delta = 20.3°$	2014-12-15-15:43:38Z + 2 weeks
* S4 +1144+40	Flaring Blazar	$\alpha = 177°, \delta = 40°$	2014-12-22-15:43:38Z + 1 weeks
* S5 +1217+71	Flaring Blazar	$\alpha = 185°, \delta = 71.1°$	2014-12-15-15:43:38Z + 2 weeks
TXS +1100+122	Flaring Blazar	$\alpha = 166°, \delta = 12.0°$	2014-12-29-15:43:38Z + 2 weeks
GRB 141221A	GRB	$\alpha = 198.3°, \delta = 8.2°$	2014-12-21-08:07:02Z $^{+1\text{day}}_{-5\text{min}}$
* GRB 141223240	GRB	$\alpha = 147.4°, \delta = -20.7°$	2014-12-23-05:45:34Z $^{+1\text{day}}_{-5\text{min}}$
GRB 141226880	GRB	$\alpha = 163.9°, \delta = 28.4°$	2014-12-26-21:07:24Z $^{+1\text{day}}_{-5\text{min}}$
GRB 141229911	GRB	$\alpha = 170.1°, \delta = 23.1°$	2014-12-29-21:51:39Z $^{+1\text{day}}_{-5\text{min}}$
* GRB 141229A	GRB	$\alpha = 72.4°, \delta = -19.2°$	2014-12-29-11:48:59 $^{+1\text{day}}_{-5\text{min}}$
GRB 141230834	GRB	$\alpha = 181.5°, \delta = 11.6°$	2014-12-30-20:00:25Z $^{+1\text{day}}_{-5\text{min}}$
GRB 141230A	GRB	$\alpha = 57.0°, \delta = 1.6°$	2014-12-30-03:24:22Z $^{+1\text{day}}_{-5\text{min}}$
GRB 150101B	GRB	$\alpha = 188.0°, \delta = -10.9°$	2015-01-01-15:23:00Z $^{+1\text{day}}_{-5\text{min}}$
GRB 150105A	GRB	$\alpha = 124.3°, \delta = -14.8°$	2015-01-05-06:10:00Z $^{+1\text{day}}_{-5\text{min}}$
GRB 150106921	GRB	$\alpha = 40.8°, \delta = 0.3°$	2015-01-06-22:05:53 $^{+1\text{day}}_{-5\text{min}}$
* SN 2014dz	SN	$\alpha = 52.1°, \delta = 38.0°$	2014-12-10-00:00:00Z + 2 weeks
SN 2014dy	SN	$\alpha = 42.2°, \delta = -0.8°$	2014-12-10-00:00:00Z + 2 weeks
* SN 2015A	SN	$\alpha = 145.3°, \delta = 35.9°$	2015-01-02-00:00:00Z + 2 weeks
SN 2015B	SN	$\alpha = 193.6°, \delta = -12.6°$	2014-12-21-00:00:00Z + 2 weeks
SN 2015D	SN	$\alpha = 198.2°, \delta = 12.6°$	2015-01-06-00:00:00Z + 2 weeks
SN 2015E	SN	$\alpha = 48.4°, \delta = 0.3°$	2014-12-31-00:00:00Z + 2 weeks
SN 2015W	SN	$\alpha = 104.4°, \delta = 13.6°$	2015-01-02-00:00:00Z + 2 weeks

Table 1. All objects considered in this search, along with coordinates and times the source is assumed to be turned on. ANITA-III launched on Dec. 18, 2014 and was terminated Jan 9, 2015. Objects with asterisks were included in the search but resulted in no passing simulated events. The times for the flaring blazar search are one-week time scales based on the Fermi telescope's elapsed mission time, hence the offset of 15:43:38 for each start time.

<div align="center">

Optimized cut values

Search	$\mathcal{F}$	$-\log_{10}\mathcal{O}$	$\mathcal{D}$	exp. ϵ	exp. backg.
TXS 0506+056	1.7	0.9	0.99	91.7%	$0.10^{+0.16}_{-0.07}$
NGC 1068	2.8	0.5	0.99	93.9%	$0.10^{+0.16}_{-0.07}$
FAVA blazars	2.3	0.9	0.96	82.2%	$0.30^{+0.25}_{-0.16}$
GRBs	1.7	0.1	0.96	92.7%	$0.10^{+0.16}_{-0.07}$
SN	2.3	0.9	0.99	93.0%	$0.23^{+0.22}_{-0.13}$

</div>

Table 2. The optimized efficiency and background for each search performed for ANITA-III. The quoted efficiency is calculated for the model used to optimize the cuts and has an estimated uncertainty of order 10%. The background is model-independent. The 16%, 50% and 84% quantiles of the posterior distribution are used to determine the central value and errors quoted.

As the best-fit spectral index of $\gamma = 3.2$ is not amenable for ANITA's sensitivity, and moreover, there is no guarantee that any particular source would have consistent spectral index over many orders of magnitude, so we set cuts by simulating neutrinos from NGC 1068 with $\gamma = 2$, resulting in an estimated analysis efficiency of 93.9% and a background of $0.10^{+0.16}_{-0.07}$ (the minimal allowed).

4.3 Flaring Blazars

Motivated in part by the apparent TXS 0506+056 flare coincidence, we consider blazars within the field of view of ANITA-III that are flaring in GeV gamma-rays as potential UHE neutrino sources. FSRQs in particular have been suggested as potential neutrino sources above 1 EeV [16, 17], although we consider all classes of blazars in this search. We use the Fermi Large Aperture Telescope's All-sky Variability Analysis (FAVA) [19] to select flaring objects labeled as blazars by 3FGL [27] during the ANITA-III flight. FAVA identifies flaring candidates on a one-week cadence, during which we assume the neutrino flux is constant.

To set cuts, we weight neutrino flux from each blazar equally. While weighting by gamma-ray flux or luminosity distance are also reasonable, equal weighting is the least model-dependent, making it less likely to miss any interesting source. As before, we assume $\gamma = 2$. The result of the optimization is an analysis efficiency estimate of 82.8% and an estimated background of $0.30^{+0.25}_{-0.16}$.

4.4 GRBs

GRBs, the brightest known transient events in the universe, have long been considered a potential source of UHE neutrinos [18, 28–31]. ANITA is most likely most sensitive to the GRB afterglow neutrino flux, which is expected to have $\gamma = 3/2$ up to some maximum energy (model-dependent, but typically order EeV).

We select GRBs from the IceCube GRBWeb catalog [32], which itself collects data from several sources [33, 34]. To optimize cuts, we chose to adopt a $\gamma = 3/2$ spectrum, typical of afterglow models, up to 10 EeV for each GRB, starting five minutes before the GRB and extending 24 hours after. While most models would not predict neutrinos up to 10 EeV for most GRBs, this choice is inclusive and will avoid missing any potential signals. This time window would also tend to accept prompt and precursor neutrinos. The period of 24 hours is chosen as a compromise between too short a window, which might reject some of the most energetic afterglow neutrinos and too long a window, which increases the possibility of

chance coincidence. The normalization of each source's flux was assumed to be proportional to the GRB fluence, using a reasonable minimum value if it is not known. Only GRBs with a declination within 30 degrees of the equator are considered. The cut optimization indicates an estimated analysis efficiency of 92.7% and the minimal possible background estimate of $0.10^{+0.16}_{-0.07}$.

4.5 Supernovae

Phenomena related to supernovae (SN) have been predicted to produce UHE neutrinos, especially in cases such as Hypernovae, magnetar-driven SN, transrelativistic SN, or tidal ignition of white dwarfs [35–40]. Despite the lack of a clear model that might produce an observable signal in ANITA, their transient nature makes them amenable to a source search. Furthermore, the upward-air shower candidate in ANITA-III was spatially coincident with Supernova 2014dz [41], which likely occurred only several days before, further motivating a search in the Askaryan channel.

Due to a lack of clear model guidance for setting cuts, we select $\gamma = 2$ and a two-week period after the estimated explosion date of the supernova, which is generally computing using spectral properties of the light curve at discovery. We select SN from the CBAT catalog [42] and do not distinguish between supernova types. Tidal disruption events (TDEs) were also considered, but none were catalogued near the time of the ANITA-III flight [43]. Optimization of cuts results in an estimated analysis efficiency of 93.0% on a background of $0.22^{+0.22}_{-0.13}$.

5 Results and Discussion

After applying the optimized cuts to each search using the procedure described above, all searches were null except for the SN search, which identified event 83134914 (Figure 5, left) as potentially associated with SN 2015D ($\mathcal{D} = 0.67$). This is consistent with the background estimate for the search ($p = 0.21$), even before accounting for the number of searches performed.

Due to a bookkeeping error in background estimation, initially a looser set of optimized cuts were computed and erroneously applied, which resulted in two additional passing events, 21318591 and 58125945 (Figure 5 center and right) that did not pass the final, corrected cuts. While these are not considered part of the result, we will comment briefly on them. All three events are summarized in Table 3.

5.1 Candidate Event 83139414

The sole candidate event this search, event 83134914, was previously identified in the ANITA-III diffuse search [6] as being neutrino-like and extremely isolated. In this search, it was found to be potentially associated with SN 2015D [44], which was discovered approximately 10 days after this event and believed to be around two weeks old at the time of discovery.

We note that that the proxy position for this event in this search ($\alpha' = 206$, $\delta' = 13.9$) differs substantially from what was reported in the diffuse search ($\alpha = 171 \pm 5$, $\delta = 16.3 \pm 1$), a position which would have failed the association cut here. The previous estimate was performed by dedicated simulations with the payload at that position, rather than the approximate method used in this paper, which is designed to reduce dispersion rather than produce a bias-free position estimator. Moreover, the handling of polarization in the simulation software has also been improved since the previous estimate was made, adding another

Details about identified events

	Candidate Ev. 83134914	Subthreshold Ev. 21318591	Subthreshold Ev. 58125945
Time	2015-01-08-19:04:24.237	2014-12-22-04:30:24Z	2015-01-01-08:17:14.615Z
Payload Pos.	70.3S, 90.1E, 33.6 km	80.2S, 82.0E, 36.6 km	76.2S, 108.6W, 34.6 km
Est. Ice Pos..	68.6S, 98.2ES	81.8S, 94.7E	74.4S, 100.3W
Proxy Sky Pos.	$\alpha' = 206°, \delta' = 13.6°$	$\alpha' = 38°, \delta' = -3.1°$	$\alpha' = 164°, \delta' = 11.7°$
Potential Associations	SN 2014 D ($\mathcal{D} = 0.67$)	4C +01.02 ($\mathcal{D} = 0.955$) NGC 1068 ($\mathcal{D} = 0.64$) SN 2014dy ($\mathcal{D} = 0.78$)	TXS 1100+122 ($\mathcal{D} = 0.003$)
$\mathcal{F}$	3.03	2.28	3.06
$-\log_{10}\mathcal{O}$	$\sim \infty$	0.41	0.68

Table 3. Details about the candidate event and subthreshold events that were associated with searches. Event 83134914 was identified by the SN search as potentially associated with SN 2015D. This event was previously identified in the diffuse ANITA-III analysis. The other two events were subthreshold but included here for completeness.

potential source of discrepancy. For the purpose of this search, the event is associated even if the localization proxy differs from the previous estimate.

This event points to isolated deep ice, very far from any known anthropogenic activity and would have passed a much more stringent isolation cut. If, hypothetically, the selection cuts were set to barely accommodate this event, the background estimate for the supernova search would be the minimal possible with the method used ($0.10^{+0.16}_{-0.07}$), which would modify the pre-trial significance of this event to $p = 0.13$. This is not enough to be interesting by itself, but is perhaps more interesting in combination with the potential association of the apparently upward air-shower in ANITA-III with an SN, which had $p = 0.0017 - 0.023$, depending on the prior used for the time dependence [41, Supplemental Material].

To get a feeling for the false association rate, should 83134914 be an anthropogenic event, we consider the sideband of VPol-identified events with $\mathcal{F} \in [1, 2]$, $-\log_{10}\mathcal{O} \in [-1, 1]$. Of these 173 sideband events, 4 (2.3%) would have passed the SN association cut value and just one event has an association as good as the candidate. 22 events (12.7%) in this sideband pass the association cut for any of the five source classes.

It is possible that 83134914 is a UHE neutrino event and not some anthropogenic background, but is associated with a SN direction by chance. By simulating a diffuse cosmogenic neutrino flux we find 10% of simulated diffuse neutrinos would be considered SN-associated in this search and 24% would be considered associated with any of the source classes at each search's cut level.

A subthreshold search in the direction of SN 2015D down to $\mathcal{F} = 0$ and $-\log_{10}\mathcal{O} = 0$ was performed, yielding one additional event. This event was isolated but was only marginally-associated with SN2014D and upon further inspection, is potentially residual radio interference from satellites.

5.2 Subthreshold Events 21318591 and 58125945

The cuts associated with the initial unblinding of the searches, which had underestimated the background estimate due to an inadvertent histogram binning mismatch, had events 21318591 and 58125945 as candidates. These events would represent the result of a valid albeit less sensitive search with slightly higher efficiency and a significantly higher (by a

factor of 2-3) background estimate. We briefly discuss these events here for completeness and transparency.

Event 21318591 was initially considered a candidate in multiple searches (NGC 1068, SN, Flaring Blazars), although, with $\mathcal{F} = 2.3$ and $-\log_{10}\mathcal{O} = 0.4$, it fails the corrected cuts for all searches. It has a much closer association to NGC 1068 ($\mathcal{D} = 0.64$) and SN ($\mathcal{D} = 0.78$, nearest SN is SN2014dy) than to the blazar search ($\mathcal{D} = 0.955$, nearest blazar is 4C +01.02). The waveform is relatively impulsive, although generally less impulsive than simulated neutrino events, but the polarization—close to equal for HPol and VPol— is atypical for a neutrino event. Moreover, a look at the closest geospatial neighboring events reveals that they have similar waveform shapes and polarization and are moreover also relatively close in time. The anthropogenic isolation cut does not consider how alike or time-correlated neighbors are (although that would be a useful future enhancement), so this additional information may qualitatively suggest an anthropogenic origin.

Event 58125945 was initially identified as very closely associated with TXS 1100+122, with the reconstructed position lying within a degree of the blazar. With $-\log_{10}\mathcal{O} = 0.7$, it (marginally) fails the corrected isolation cut. This event is extremely impulsive and is virtually purely VPol, but appears to point to thin ice within Pine Island Glacier, a part of the continent with relatively low likelihood to produce detectable Askaryan neutrino events. Over the pointing uncertainty of the event, the ice thickness varies from sea ice to 1.2 km. Pine Island Glacier is one of the warmest parts of the ice sheet, implying relatively high radio attenuation in its ice. This event is somewhat isolated, but its nearest neighbors, which themselves form a cluster of dozens of events, are similarly impulsive and also mostly VPol. We cannot rule out that this event is a pointing reconstruction outlier from this larger cluster. The British Antarctic Survey was conducting radar and drilling studies in Pine Island Glacier during the 2014-2015 season [45], however due to a powerful storm on January 1, there was no significant activity during the time of the event [46]. The powerful storm additionally admits the possibility of triboelectric emission [47].

Despite these significant caveats, due to the apparent close association with TXS 1100+122, a review of the astrophysical literature on this object is worth presenting. TXS 1100+122 was first observed in gamma-rays [48] in a 2013 flare, followed by the early January 2015 [49] flare detected by FAVA and therefore entering this object into this analysis. The gamma-ray flare had a hard spectrum and was coincident with an optical flare of two magnitudes. More recently, TXS 1100+122 has been suggested as a potentially interesting neutrino source [50], on the basis of TXS 1100+122 being compatible in position with IceCube alert event (IC-200109A [51]) and possessing a compact radio emission core, a feature suggested as possibly being associated with neutrino emission [52].

5.3 Limits

As we do not find any significant associations, we proceed to set upper limits on fluence during the ANITA-III flight from each source. Model-independent limits on fluence at a given energy $\Phi(E)$ are given by

$$u.l.(E^2\Phi(E)) = \left\langle \frac{FC_{90}(n_{obs}, \mu_{bg}) \cdot E}{\epsilon A_{eff}(E) \cdot \Delta} \right\rangle, \tag{5.1}$$

where Δ is a factor compensating for the use of discrete energies, while the flux and acceptance both evolve continuously. ANITA cosmogenic searches have typically used $\Delta = 4$ [20], based on studies showing that this is a reasonable choice for a variety of models [53]. We
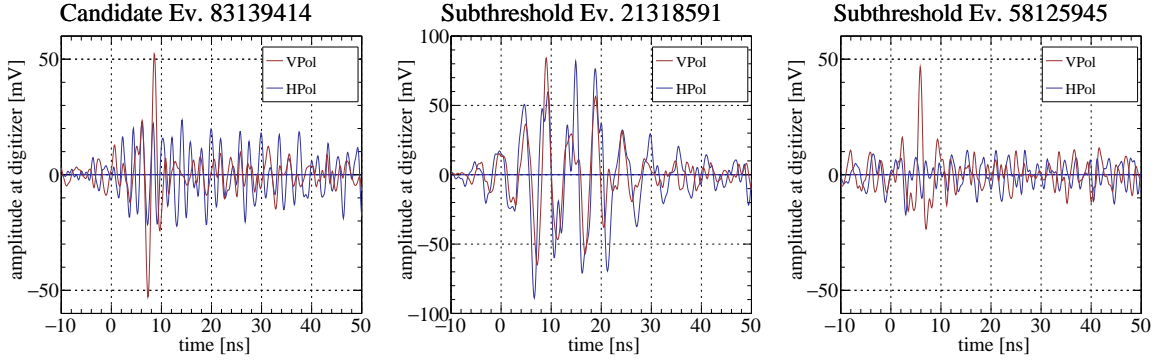
Figure 5. The candidate event (left) and two subthreshold events identified in this analysis. These waveforms represent a coherent sum based on the estimated radio direction and with the group delay from filters and antennas removed.

maintain this convention here for consistency, but note that other experiments use different conventions.

For objects in source classes with multiple members, setting a limit is slightly more involved. While it is straightforward to calculate the effective area and efficiency given the cuts for each source within the class, partitioning the background estimate is somewhat more complex, as the background estimate was assigned for the entire class, not any particular object. However, assuming zero background for the purpose of setting limits on each source will produce conservative upper limits with small error. The true answer is bounded by ascribing zero background to a source and ascribing the total background of the source class to a source, and this difference is small ($\mathcal{O}(10\%)$) in all cases. Upper limits for each source are shown in Figure 6. Some sources are omitted due to a paucity of simulated triggered events or low analysis efficiency.

In addition to model-independent energy-dependent limits, we show integrated $\gamma = 2$ limits for AGN-like and SN searches, where the upper limit on normalization for a $\Phi(E) = \Phi_0(E^{-2})$ is calculated using:

$$u.l.(\Phi_0) = \left\langle \frac{FC_{90}(n_{obs}, \mu_{bg}) \cdot \phi_0}{\langle \epsilon \cdot A_{eff}(E) \rangle \mid_{\phi(E)}} \right\rangle, \tag{5.2}$$

where A_{eff} and ϵ are averages over the unity-normalized flux $\phi(E) = \phi_0 E^{-2}$, with $\phi_0 = 1.00$ EeV for the energy range considered.

The measured fluence for the apparent 2014-2015 TXS 0506+056 neutrino flare from IceCube was $E^2\Phi(E) = (0.21^{+0.09}_{-0.07})$ GeVcm$^{-2}(E/10^5\text{GeV})^{2-2.1\pm0.2}$ over a Gaussian window centered on 2014-12-14±14 days with a width of 110^{+34}_{-24} days [14]. The ANITA-III flight time represents a fraction of 0.16 of this time window. This fluence band, scaled to the ANITA-III flight time, is projected onto the top-left panel of Figure 6.

6 Conclusion and Outlook

We find that there is no significant evidence for any source-associated neutrinos with ANITA-III, although the potential SN association of the ANITA-III diffuse analysis event is somewhat intriguing, especially in combination with previous results. Given that the analysis efficiency of the ANITA-III diffuse search was quite high, this is perhaps not too surprising a result, as
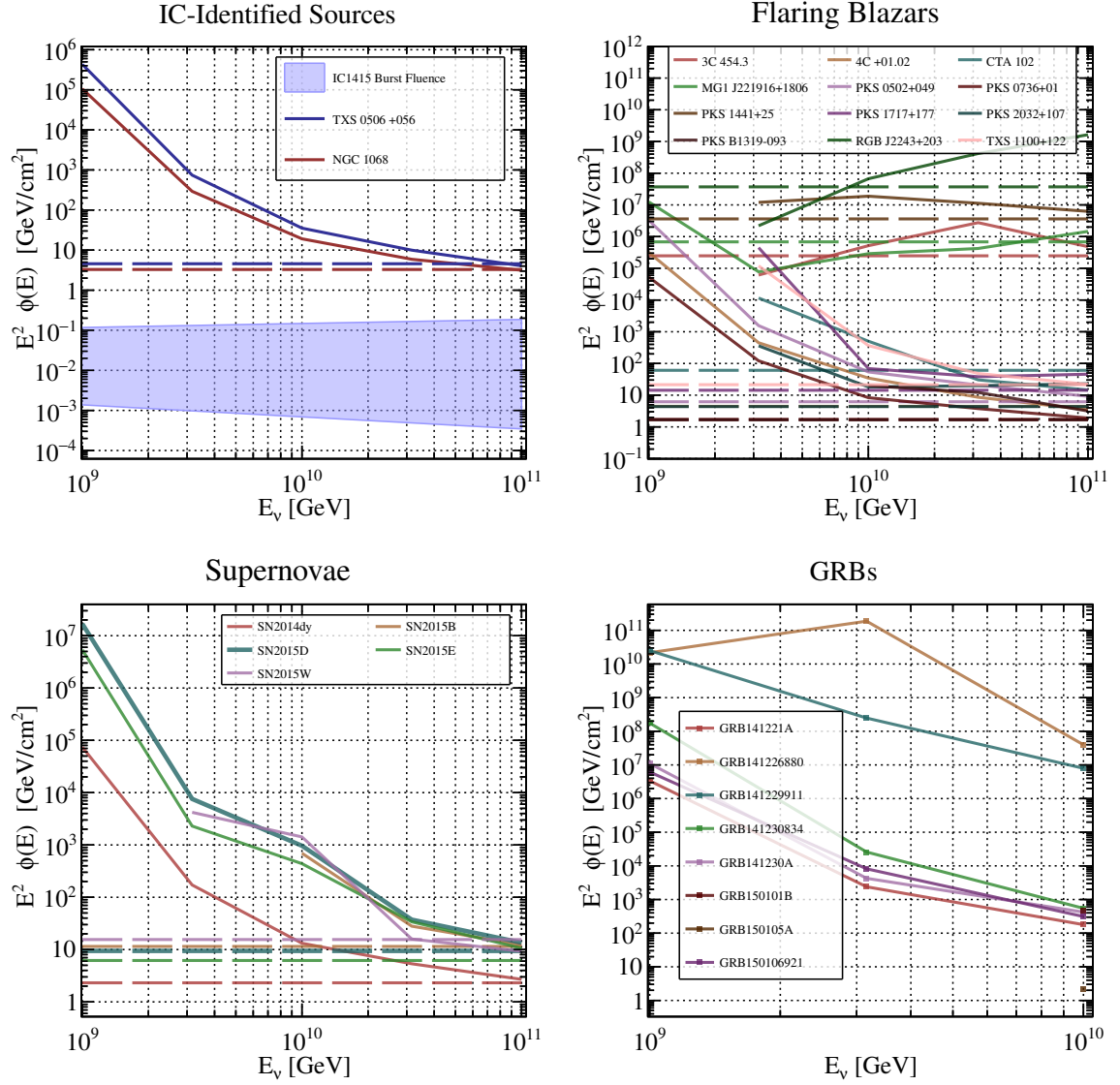
Figure 6. ANITA-III limits on neutrino fluence for all objects considered in these searches. The top-left panel shows fluence limits on TXS 0506+056 and NGC 1068, along with the extrapolated time-scaled fluence from the 2014-2015 apparent IceCube neutrino burst in the direction of TXS 0506+056. The top right shows fluence limits flaring blazars that result in triggered simulated events (points are not shown at energies with no simulated passing events). Some blazars (e.g RBG J2243+203) suffer from poor geometry. The bottom left shows fluence limits on SN and the bottom right shows fluence limits on GRBs. Model-independent limits are shown with solid lines and integrated E^{-2} limits are shown with dashed lines, where appropriate.

there is relatively little phase space for neutrinos that would trigger ANITA-III but not pass diffuse analysis cuts. As evinced by the subthreshold events identified, further loosening the cuts does lead to additional events, but the higher background limits the discovery potential. Still, using this methodology we are able to set limits on individual sources, which could not be done coherently in the diffuse search. A similar search is in progress for the more recent and more sensitive ANITA-IV payload.

The discovery potential of the methods described here would be improved in cases where there is additional room between the trigger efficiency and diffuse-search analysis efficiency, suggesting that it is still advantageous to reduce trigger thresholds significantly below the effective analysis threshold for a diffuse search. This could not be achieved in ANITA-III as the acquisition system could not handle the increased data rate from significantly reducing the trigger threshold. Moreover, significant effort in thermal noise reduction and spatial clustering was able to substantially improve the analysis efficiency compared to ANITA-I and ANITA-II. However, a significant gap between analysis and trigger efficiency currently exists in some current in-ice UHE neutrino experiments, such as ARA [54], which could benefit from an adaptation of the methods described here. Future UHE neutrino detectors using the Askaryan method such as PUEO [55], RNO-G [56], or the radio extension of IceCube-Gen2 [57] may also benefit from similar methods if the trigger threshold can be made sufficiently low.

The method outlined here suffers from an inability to reduce background below some level, due to the use of a sideband for background estimation. Finding additional handles on background would also help to improve the sensitivity. This may be accomplished through improved modeling of anthropogenic backgrounds (easier in the case of fixed-position detectors) or through the use of sidebands with relatively more phase space (for example, by further tightening the angular reconstruction or introducing additional variables). With the minimal background estimate achievable in this analysis, four events are necessary for $> 3\sigma$ evidence and eight events would be required for $> 5\sigma$ discovery, before accounting for trials factors. Doubling the relative size of the sideband, for example, would reduce the number of events required to exceed each significance threshold by one. We note that the planned PUEO mission is projected to be more than an order of magnitude more sensitive than ANITA-III, implying that a transient fluence producing one event in ANITA-III would likely yield a statistically-significant excess in PUEO.

Acknowledgments

References

[1] ANITA collaboration, *The Antarctic Impulsive Transient Antenna ultra-high energy neutrino detector: Design, performance, and sensitivity for the 2006-2007 balloon flight*, *Astropart. Phys.* **32** (2009) 10 [0812.1920].

[2] G. Askaryan, *Excess negative charge of an Electron-photon shower and its coherent radio emission*, *Sov. Phys. JETP* **14 (2)** (1962) 441.

[3] ANITA collaboration, *Observations of the Askaryan effect in ice*, *Phys. Rev. Lett.* **99** (2007) 171101 [hep-ex/0611008].

[4] ANITA collaboration, *New Limits on the ultra-high energy cosmic neutrino flux from the ANITA experiment*, *Phys. Rev. Lett.* **103** (2009) 051103 [0812.2715].

[5] ANITA collaboration, *Observational constraints on the ultra-high energy cosmic neutrino flux from the second flight of the ANITA experiment*, *Phys. Rev. D* **82** (2010) 022004.

[6] ANITA collaboration, *Constraints on the diffuse high-energy neutrino flux from the third flight of ANITA*, *Phys. Rev. D* **98** (2018) 022001 [1803.02719].

[7] ANITA collaboration, *Constraints on the ultrahigh-energy cosmic neutrino flux from the fourth flight of ANITA*, *Phys. Rev. D* **99** (2019) 122001 [1902.04005].

[8] ANITA collaboration, *The First Limits on the Ultra-high Energy Neutrino Fluence from Gamma-ray Bursts*, *Astrophys. J.* **736** (2011) 50 [1102.3206].

[9] K. Greisen, *End to the cosmic ray spectrum?*, *Phys. Rev. Lett.* **16** (1966) 748.

[10] G. Zatsepin and V. Kuzmin, *Upper limit of the spectrum of cosmic rays*, *JETP Lett.* **4** (1966) 78.

[11] K. Kotera, D. Allard and A.V. Olinto, *Cosmogenic neutrinos: parameter space and detectabilty from PeV to ZeV*, *J. Cosmol. Astropart. Phys.* **10** (2010) 13 [1009.1382].

[12] IceCube collaboration, *Evidence for high-energy extraterrestrial neutrinos at the icecube detector*, *Science* **342** (2013) [1311.5238].

[13] IceCube, Fermi-LAT, MAGIC, AGILE, ASAS-SN, HAWC, H.E.S.S., INTEGRAL, Kanata, Kiso, Kapteyn, Liverpool Telescope, Subaru, Swift NuSTAR, VERITAS, VLA/17B-403 collaboration, *Multimessenger observations of a flaring blazar coincident with high-energy neutrino IceCube-170922A*, *Science* **361** (2018) eaat1378 [1807.08816].

[14] IceCube collaboration, *Neutrino emission from the direction of the blazar TXS 0506+056 prior to the IceCube-170922A alert*, *Science* (2018) eaat2890 [1807.08794].

[15] IceCube collaboration, *Time-Integrated Neutrino Source Searches with 10 Years of IceCube Data*, *Phys. Rev. Lett.* **124** (2020) 051103 [1910.08488].

[16] C. Righi et al., *EeV Astrophysical neutrinos from FSRQs?*, 2003.08701.

[17] X. Rodrigues et al., *Blazar origin of the UHECRs and perspectives for the detection of astrophysical source neutrinos at EeV energies*, 2003.08392.

[18] E. Waxman and J.N. Bahcall, *Neutrino afterglow from gamma-ray bursts:* $\sim 10^{18}$-*eV*, *Astrophys. J.* **541** (2000) 707 [hep-ph/9909286].

[19] S. Abdollahi et al., *The Second Catalog of Flaring Gamma-Ray Sources from the Fermi All-sky Variability Analysis*, *Astrophys. J.* **846** (2017) 34 [1612.03165].

[20] ANITA collaboration, *The Simulation of the Sensitivity of the Antarctic Impulsive Transient Antenna (ANITA) to Askaryan Radiation from Cosmogenic Neutrinos Interacting in the Antarctic Ice*, *JINST* **14** (2019) P08011 [1903.11043].

[21] P. Fretwell et al., *Bedmap2: improved ice bed, surface and thickness datasets for antarctica*, *Cryosphere* **7** (2013) 375.

[22] A. Hoecker et al., *TMVA - Toolkit for Multivariate Data Analysis*, *PoS* **ACAT2007** (2007) 040 [physics/0703039].

[23] G.J. Feldman and R.D. Cousins, *A Unified approach to the classical statistical analysis of small signals*, *Phys. Rev. D* **57** (1998) 3873 [physics/9711021].

[24] R.D. Cousins and V.L. Highland, *Incorporating systematic uncertainties into an upper limit*, *Nucl. Instrum. Meth. A* **320** (1992) 331.

[25] T.P. Li and Y.Q. Ma, *Analysis methods for results in gamma-ray astronomy.*, *Astrophys. J.* **272** (1983) 317.

[26] P. Padovani et al., *Dissecting the region around IceCube-170922A: the blazar TXS 0506+056 as the first cosmic neutrino source*, *Monthly Notices of the Royal Astronomical Society* **480** (2018) 192–203 [1807.04461].

[27] FERMI-LAT collaboration, *Fermi Large Area Telescope Third Source Catalog*, *Astrophys. J. Suppl.* **218** (2015) 23 [1501.02003].

[28] K. Murase, *High energy neutrino early afterglows gamma-ray bursts revisited*, *Phys. Rev.* **D76** (2007) 123001 [0707.1140].

[29] E. Waxman and J.N. Bahcall, *High-energy neutrinos from cosmological gamma-ray burst fireballs*, *Phys. Rev. Lett.* **78** (1997) 2292 [astro-ph/9701231].

[30] S. Razzaque and L. Yang, *PeV-EeV neutrinos from GRB blast waves in IceCube and future neutrino telescopes*, *Phys. Rev. D* **91** (2015) 043003 [1411.7491].

[31] J.K. Thomas, R. Moharana and S. Razzaque, *Ultrahigh energy neutrino afterglows of nearby long duration gamma-ray bursts*, *Phys. Rev. D* **96** (2017) 103004 [1710.04024].

[32] P. Coppin, *GRBWeb*, 2020. https://icecube.wisc.edu/~grbweb_public/.

[33] A. Lien et al., *The Third Swift Burst Alert Telescope Gamma-Ray Burst Catalog*, *Astrophys. J.* **829** (2016) 7 [1606.01956].

[34] A. von Kienlin et al., *The fourth Fermi-GBM gamma-ray burst catalog: A decade of data*, *The Astrophysical Journal* **893** (2020) 46 [2002.11460].

[35] X.-Y. Wang, S. Razzaque, P. Meszaros and Z.-G. Dai, *High-energy Cosmic Rays and Neutrinos from Semi-relativistic Hypernovae*, *Phys. Rev. D* **76** (2007) 083009 [0705.0027].

[36] B.T. Zhang and K. Murase, *Ultrahigh-energy cosmic-ray nuclei and neutrinos from engine-driven supernovae*, *Phys. Rev. D* **100** (2019) 103004 [1812.10289].

[37] K. Murase, P. Meszaros and B. Zhang, *Probing the birth of fast rotating magnetars through high-energy neutrinos*, *Phys. Rev. D* **79** (2009) 103001 [0904.2509].

[38] D. Biehl, D. Boncioli, C. Lunardini and W. Winter, *Tidally disrupted stars as a possible origin of both cosmic rays and neutrinos at the highest energies*, *Sci. Rep.* **8** (2018) 10828 [1711.03555].

[39] R. Alves Batista and J. Silk, *Ultrahigh-energy cosmic rays from tidally-ignited white dwarfs*, *Phys. Rev. D* **96** (2017) 103003 [1702.06978].

[40] K. Murase, *New Prospects for Detecting High-Energy Neutrinos from Nearby Supernovae*, *Phys. Rev. D* **97** (2018) 081301 [1705.04750].

[41] ANITA collaboration, *Observation of an unusual upward-going cosmic-ray-like event in the third flight of anita*, *Phys. Rev. Lett.* **121** (2018) 161102.

[42] CBAT, *CBAT SN catalog*, 2015.

[43] J. Guillochon, *Open TDE catalog*, 2020. http://TDE.space.

[44] Z.w. Jin et al., *Supernova 2015D in NGC 5020 = Psn J13124116+1236018*, *Central Bureau Electronic Telegrams* **4051** (2015) 1.

[45] R. Mulvaney and A.M. Smith, *Borehole derived pine island glacier mean annual temperatures*, *NERC Polar Data Centre* (2017) .

[46] R. Mulvaney. Private Communication, 2020.

[47] ANITA collaboration, *Experimental tests of sub-surface reflectors as an explanation for the ANITA anomalous events*, 2009.13010.

[48] R. Ojha, B. Carpenter and C.C. Cheung, *Fermi LAT Detection of a GeV flare from spectrally hard FSRQ TXS 1100+122*, *The Astronomer's Telegram* **5202** (2013) 1.

[49] T. Pursimo, R. Ojha and D. Kocevski, *Optical and Gamma-ray Flare from spectrally hard FSRQ TXS 1100+122*, *The Astronomer's Telegram* **6914** (2015) 1.

[50] Y.Y. Kovalev et al., *Flat spectrum radio quasar TXS 1100+122 has a bright VLBI-compact core - as expected for neutrino candidate sources*, *The Astronomer's Telegram* **13397** (2020) 1.

[51] IceCube collaboration, *IceCube-200109A: IceCube observation of a high-energy neutrino candidate event*, *GRB Coordinates Network* **26696** (2020) 1.

[52] A. Plavin, Y. Kovalev, Y. Kovalev and S. Troitsky, *Observational evidence for the origin of high-energy neutrinos in parsec-scale nuclei of radio-bright active galaxies*, *Astrophys. J.* **894** (2020) 101 [2001.00930].

[53] I. Kravchenko et al., *RICE limits on the diffuse ultrahigh energy neutrino flux*, *Phys. Rev. D* **73** (2006) 082002 [astro-ph/0601148].

[54] ARA collaboration, *Constraints on the diffuse flux of ultrahigh energy neutrinos from four years of askaryan radio array data in two stations*, *Phys. Rev. D* **102** (2020) 043021 [1912.00987].

[55] PUEO collaboration, *The Payload for Ultrahigh Energy Observations (PUEO): A white paper*, 2010.02892.

[56] RNO-G collaboration, J. Aguilar et al., *Design and sensitivity of the Radio Neutrino Observatory in Greenland RNO-G*, 2020. Under preparation.

[57] IceCube Gen2 collaboration, *IceCube-Gen2: The Window to the Extreme Universe*, 2008.04323.

[58] F. Rademakers et al., *root-project/root: v6.18/02*, Aug., 2019. 10.5281/zenodo.3895860.

[59] R. Brun and F. Rademakers, *ROOT: An object oriented data analysis framework*, *Nucl. Instrum. Meth. A* **389** (1997) 81.